Assessing Raindrop Breakup Parameterizations Using Disdrometer Observations

STEPHEN M. SALEEBY,[a] BRENDA DOLAN,[a] JENNIE BUKOWSKI,[a] KRISTEN VAN VALKENBURG,[a] SUSAN C. VAN DEN HEEVER,[a] AND STEVEN A. RUTLEDGE[a]

[a] *Department of Atmospheric Science, Colorado State University, Fort Collins, Colorado*

(Manuscript received 21 December 2021, in final form 30 June 2022)

ABSTRACT: An intercomparison of raindrop mean diameter frequency distribution (RDFD) is performed for numerical simulations of precipitating cloud systems using an array of models and microphysics schemes. This includes results from the Regional Atmospheric Modeling System (RAMS) double-moment microphysics, the Hebrew University Cloud Model bin microphysics (HUCM) interfaced to the RAMS parent model, and the Weather Research and Forecasting (WRF) Model with the Thompson, Morrison, double-moment 6-class (WDM6), and National Severe Storms Laboratory (NSSL) double-moment schemes. Simulations are examined with respect to the raindrop size distribution (DSD) volume-number mean diameter (D_m) and intercept parameter (N_w). When compared to a suite of disdrometer observations, the RDFD resulting from each microphysics scheme exhibits varying degrees of mean drop size constraints and peaks in the frequency distribution of D_m. A more detailed investigation of the peaked RDFD from the RAMS simulations suggests that the parameterization of raindrop collisional breakup can impose strong limitations on the evolution of simulated drop growth. As such, a summary and comparison of the drop breakup parameterizations among the aforementioned microphysics schemes is presented. While some drop breakup parameterizations are adjusted toward the observations by modifying the threshold diameter for the onset of breakup, this study explores the use of a modified maximum breakup efficiency. This method permits the parameterization to retain its threshold breakup diameter, while limiting the strength of drop breakup and permitting a broader range of drop sizes. As a result, the simulated mean drop sizes are in better agreement with observations.

KEYWORDS: Cloud parameterizations; Cloud resolving models; Model evaluation/performance

1. Introduction

Accurate prediction and representation of the raindrop size distribution (DSD) in the microphysical schemes of numerical weather prediction models is essential for accurately representing cloud and precipitation processes. To this end, numerous methods have been developed to simulate the initial formation of the DSD via cloud droplet autoconversion and raindrop accretion processes, some of which use bulk distribution (Berry and Reinhardt 1974, hereafter BR74) bin-emulating (Tzivion et al. 1987; Meyers et al. 1997), or spectral-bin approaches (Khain et al. 2004). Bulk hydrometeor distribution and bin-emulating approaches assume a priori size distributions of hydrometeors, typically with an exponential or gamma distribution shape, while a computationally demanding spectral-bin approach permits the evolution of the size distribution with no assumed shape. There are various advantages and disadvantages to using these different approaches, the assessment of which is further complicated by the fact that they function alongside processes such as drop sedimentation, drop self-collection, and ice processes of raindrop production (via melting and shedding) for generating a representative DSD (e.g., Meyers et al. 1997; Morrison et al. 2009; Thompson et al. 2008; Khain et al. 2004). The synergy of these parameterized processes ultimately determines the prognosis of liquid water content (LWC), number concentration (N_r), and diameter of raindrops, with significant implications for research and forecasting applications.

Most microphysics schemes have parameters that are adjusted to permit better agreement between simulated and observed DSDs, as well as other hydrometeor quantities. This requires setting parameters within an acceptable physical range, while adjusting them to operate appropriately within the overarching microphysics scheme. As such, there are often multiple microphysics schemes using the same parameterization basis functions to represent processes such as raindrop collisional breakup, but that utilize model-customized coefficients that are calibrated to produce the most representative DSDs (Meyers et al. 1997; Thompson et al. 2004, 2008; Morrison et al. 2009, 2012; Lim and Hong 2010). Variations in such parameterization coefficients within a common parent microphysics scheme have been demonstrated to result in very different solutions due to complex nonlinear interactions of parameterized microphysical processes. As such they may benefit from calibration to improve their agreement with observations (Morrison et al. 2012; Planche et al. 2019).

One such microphysical process that has undergone parameterization adjustments and tuning in numerical models is that of raindrop collisional breakup (Ziegler 1985; Meyers et al. 1997; Khain et al. 2004; Thompson et al. 2004, 2008; Morrison et al. 2009, 2012; Lim and Hong 2010; Mansell et al. 2010). There is a general lack of theoretical formulations upon which to base the development of a rigorous parameterization for drop breakup. Seifert et al. (2005) note that models largely rely upon 1) parameterizations that seek to generate equilibrium DSDs that generally agree with observations, such as the use of DSDs from Zawadzki and de Agostino Antonio (1988, hereafter ZA88) in the formulation of

Corresponding author: Stephen M. Saleeby, stephen.saleeby@colostate.edu

DOI: 10.1175/JAS-D-21-0335.1

TABLE 1. Simulations used for comparisons in this study.

Name	Regime	Idealized or case	Comments	References
Supercell	CM	Idealized	Dx = 300	Grant and van den Heever (2014a)
MC3E	CM	Case study	20 May 2011 squall line	Marinescu et al. (2016)
ATEX	OM	Idealized	Shallow stratocumulus, warm rain only	Saleeby et al. (2015)
BSISO1	OT	Case study	Phase 01 inactive	Toms et al. (2020)
BSISO2	OT	Case study	Phase 02 inactive	Toms et al. (2020)
BSISO6	OT	Case study	Phase 06 more active	Toms et al. (2020)
BSISO8	OT	Case study	Phase 08 less active	Toms et al. (2020)
Deep Tropical NoDust	OT	Idealized	Isolated deep convection	Saleeby et al. (2011)
Deep Tropical CCN	OT	Idealized	Isolated deep convection: DUST CCN + IN	Saleeby et al. (2011)
Deep Tropical Dust	OT	Idealized	Isolated deep convection: Dust IN only	Saleeby et al. (2011)
Tropical Linear	OT	Idealized—RCE	RCE linear convection	Grant et al. (2018)
Tropical Cluster	OT	Idealized—RCE	RCE cluster convection	Grant et al. (2018)
Sea breeze Polluted	CT	Idealized	Polluted sea breeze	Grant and van den Heever (2014b)
Sea breeze Control	CT	Idealized	Control CCN sea breeze	Grant and van den Heever (2014b)

Verlinde and Cotton (1993, hereafter VC93), or 2) data from the few laboratory studies of breakup (e.g., Pruppacher and Klett 1997; Low and List 1982, hereafter LL82). More recent laboratory observations (e.g., Barros et al. 2008) and refinements to the LL82 parameterization (e.g., McFarquhar 2004; Straub et al. 2010; Schlottke et al. 2010; Prat et al. 2012) have improved upon LL82 by extrapolating to more numerous drop-pair collisions, permitting drop eccentricity, and/or utilizing more updated collision kernels, among other things. Some of these refined parameterizations produce rain DSDs that tend to vary in the resulting number concentrations of drops toward the tails of the distribution compared to LL82. As such, many of these studies highlight the need for more robust laboratory work and observations on which to base a more theoretically formulated parameterization of drop collisions and breakup. Recent modeling studies have demonstrated that some microphysics schemes overpredict raindrop size and underpredict number concentration for differing reasons. It has been demonstrated that models directly benefit from adjustments to the drop breakup equations to modify collisional breakup, thereby producing DSDs in better agreement with their observations (Morrison et al. 2012; Planche et al. 2019).

Dolan et al. (2018) presented a method of examining DSDs from global disdrometer data via the use of typical disdrometer-derived quantities by applying statistical analysis techniques. They synthesized disdrometer data from an array of field projects, spanning various global locations, and presented the results in $\log N_w$–D_0 phase space, where N_w ($\mathrm{mm^{-1}\ m^{-3}}$) is the intercept parameter of the normalized raindrop gamma distribution given as

$$N_w = \frac{3.67^4\ 10^3\ \mathrm{LWC}}{\pi \rho_w D_0^4}, \tag{1}$$

where D_0 (mm) is the median volume raindrop diameter, LWC ($\mathrm{g\ cm^{-3}}$) is liquid water content, and ρ_w ($\mathrm{g\ cm^{-3}}$) is water density. The extensive disdrometer database in $\log N_w$–D_0 phase space is shown in Fig. 12 of Dolan et al. (2018).

We note here that the disdrometer observations are subject to the detection capabilities, sampling limitations, and quality control of the disdrometer datasets used. As discussed by Dolan et al. (2018), disdrometers such as 2DVD's have difficulty measuring the smallest drops (<0.3 mm; Tokay et al. 2001), and the quality control process limits data in the smallest bin as well as samples with fewer than 100 drops in order to account for splashing, drop shatter, insects, and drop shadowing (Tokay et al. 2001; Thompson et al. 2015). Additionally, disdrometers likely undersample large drops (>5 mm) due to the small catchment cross section combined with the infrequency of drops of such sizes (Smith et al. 1993; Gatlin et al. 2015). The distribution of individual drops measured by the disdrometers are fit to a distribution with a given D_0.

In this study we utilize an extensive archive of simulations, produced from the Regional Atmospheric Modeling System (RAMS) (Cotton et al. 2003), using two-moment bulk microphysics (Verlinde et al. 1990; Walko et al. 1995; Meyers et al. 1997; Walko et al. 2000; Saleeby and Cotton 2004; Saleeby and van den Heever 2013) to perform a similar statistical analysis of rain DSDs as was done for the suite of global disdrometer data by Dolan et al. (2018). Like the disdrometer data suite, the simulation archive covers a variety of precipitation systems ranging from continental to maritime systems and from warm-phase to mixed-phase systems as shown in Table 1. We seek to determine if this large sample of model-generated rain DSDs exhibits a similar raindrop mean diameter frequency distribution compared to the global disdrometer data while considering the limitations and numerical constraints within both the models and observations (e.g., disdrometers have minimum size and number detection thresholds for reliable results and models have parameterized numerical bounds and limits).

Within the RAMS microphysics model, the hydrometeor size distributions are represented by gamma functions that require an a priori choice of the distribution shape parameter. For speed of computation, most parameterizations in RAMS, including the raindrop breakup formulation, rely on precomputed

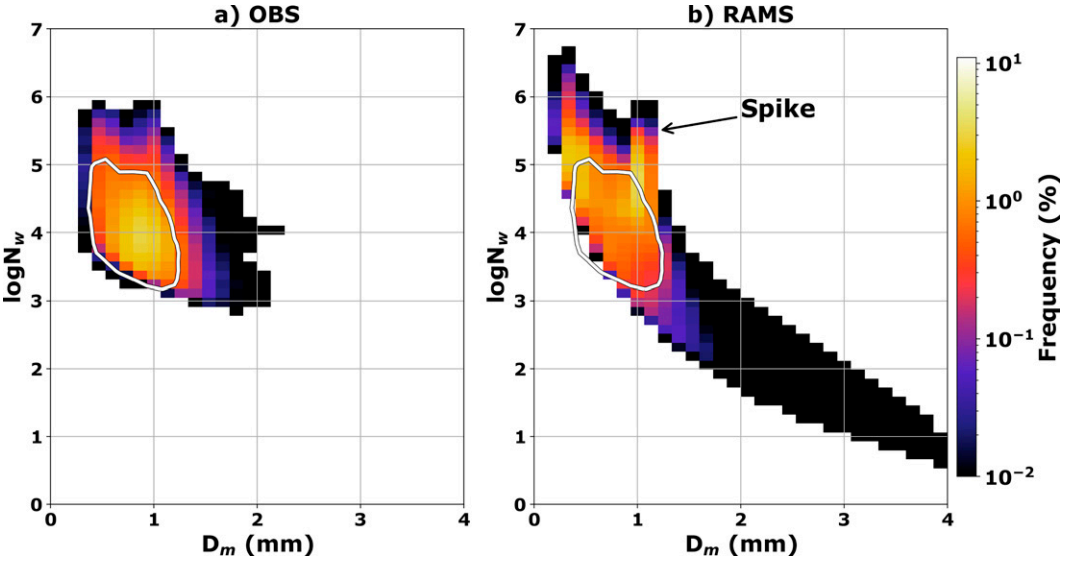

FIG. 1. Raindrop mean diameter frequency distributions expressed in logN_w–D_m phase space from (a) global surface disdrometer data (from Dolan et al. 2018) and (b) RAMS simulation data with a reference frequency contour from (a) overlaid. The distinct peak seen for large logN_w near $D_m \sim 1$ mm, which is discussed in the text, is noted by the arrow and "spike" label and is referred to as the "spike" throughout the text.

normalized gamma functions and the readily computed diameter of the mean mass, D_m. This D_m can be calculated directly from the total hydrometeor mass (q_r) and number (N_r) mixing ratios, via a power-law function, without the need for iterating over the full gamma distribution. Further, this same D_m can also be computed from the gamma distribution number spectrum as the ratio of the third moment to the zeroth moment and may be referred to as the "volume-number mean diameter." For a direct comparison between the model data in this study and the disdrometer data discussed in Dolan et al. (2018) we have computed this D_m for all of the model and disdrometer rain DSDs presented in this study. This provides a common representative distribution drop diameter, in which to compare the disdrometer and model data, that is anchored to the raindrop distribution representative diameter used by the RAMS microphysics scheme. As such, for the remainder of the manuscript, D_m refers to the "volume-number mean diameter," and the associated N_w is computed from this D_m similar to Eq. (2) below from Williams et al. (2014):

$$N_w = \frac{4^4\ 10^3\ LWC}{\pi \rho_w D_m^4}. \tag{2}$$

After adapting the disdrometer and model data to the same raindrop distribution framework, we see in Fig. 1 that the RAMS-simulated DSDs are in general agreement with the disdrometer observations with respect to the peak frequencies of occurrence residing inside the white contour line in Figs. 1a and 1b. This is quite encouraging and indicates that the model is generally doing quite well in representing the most frequent rain DSD size and number across an array of simulated environments. However, there are several noticeably different features in the simulated phase space: 1) the distinct spike that occurs for large logN_w near $D_m \sim 1$ mm, 2) the long tail of the D_m distribution for $D_m > 2.0$ mm, and 3) the lower frequency of occurrence of drops with D_m between 1.0 and 1.5 mm. The lack of a long tail in the disdrometer data is likely related to the sampling limitations discussed above, and thus, we will not address this further. However, the unusual spike seen in the analysis of the RAMS simulations (Fig. 1b) is quite prominent and is not apparent in the disdrometer observational analysis. We speculate that this feature is the result of a particular parameterization used to simulate a microphysical process. Finally, it is hypothesized that the lesser frequency of occurrence of modeled rain DSD with $D_m > 1$ mm at lower logN_w is associated with the spike in smaller drops of ~1 mm size. For the remainder of this study the spike or peak at log$N_w > 5$ and $D_m \sim 1$ mm will be referred to as the "spike." After identifying the spike near 1 mm in the composite simulation analysis, the same analysis was repeated individually for every simulation comprising the composite shown in Fig. 1b.

This analysis demonstrated that the spike was more prevalent in deep convective simulations, compared to shallow convection, due to the presence of larger sized drops that are subject to breakup. As such, the investigation presented here will focus solely on the supercell case from the simulation archive. Given the noted differences between the disdrometer observations and simulated rain distributions, this paper presents an investigation to 1) determine the cause of the prominent spike and the dominant frequency of occurrence of drop DSD with $D_m \sim 1$ mm, 2) compare representative raindrop D_m frequency distributions produced from a suite of different microphysics schemes, and 3) present a generalized method of adjusting raindrop breakup parameterizations aimed at bringing simulated rain DSDs and observations into better agreement.

TABLE 2. Summary of model grid setup and simulation configuration.

Model aspect	Setting
Horizontal grid	300 m horizontal spacing
	950 × 750 horizontal grid points
Vertical grid	92 vertical levels
	Δz = 50 m lowest level stretched to 500 m aloft
	Model top at ~22 km AGL
Initialization	Horizontally homogeneous supercell; sounding profile of Grant and van den Heever (2014a)
	2 K near-surface thermal perturbation
Boundary conditions	Radiative lateral boundaries, no surface fluxes, Rayleigh friction damping from 20 to 22 km aloft
Radiation	None
Coriolis	None
Duration	3 h at 1 s time step
Turbulence scheme	Smagorinsky (1963)
Microphysics scheme	RAMS two-moment bulk (Meyers et al. 1997)

2. Results from supercell simulation

The RAMS-simulated supercell case was initialized with a modified Weismann–Klemp sounding as depicted by Grant and van den Heever (2014a). Additional details of this simulation are provided in Table 2. The simulated storm undergoes multiple splitting and generates rainfall in both the left and right mover cells, as seen in Fig. 2a. The associated plot of the raindrop D_m frequency distribution in logN_w–D_m phase space is shown in Fig. 2b. A comparison of the plots of logN_w–D_m between Fig. 2b and Fig. 1b demonstrate that the supercell simulation produces a similar D_m distribution compared to the full simulation archive, and the spike is clearly present. The spike at $D_m \sim 1$ mm indicates a propensity for raindrop D_m to cluster at this size over a wide range of high logN_w. This suggests that the microphysics parameterization responsible for this feature tends to generate drops of a specific D_m.

To examine the frequency of occurrence of a particular D_m, the corresponding near-surface raindrop D_m frequency distribution (RDFD) is shown in Fig. 3. The D_m values were separated into 0.04 mm bins, and each grid cell in the lowest model layer containing rain mixing ratio of at least 0.01 g kg^{-1} was included for the duration of the simulation. Most of the sampled grid cells, regardless of rain LWC or number concentration, fall within a narrow range centered near 1 mm. While the dominant spike near 1 mm remains the focus of this paper, since it is associated with the clearest anomalous feature in comparison to the disdrometer observations, there is also a secondary a peak near 0.7 mm. It is suspected that the lesser peak is associated with either warm phase collision–coalescence growth of drops or melting of smaller ice particles.

To isolate the parameterization(s) responsible for this distinct D_m peak near 1 mm diameter, we performed an exhaustive set of additional supercell test simulations, with various microphysical parameterizations either turned on and off or with modified parameterization coefficients. From these tests, only modification or exclusion of the raindrop self-collection process led to a reduced or eliminated spike at $D_m \sim 1$ mm. More specifically, the spike is directly linked to the representation of raindrop self-collisional breakup. While other processes, such as autoconversion, accretion, drop shedding of hail, and melting of ice (e.g., Brown et al. 2017) certainly

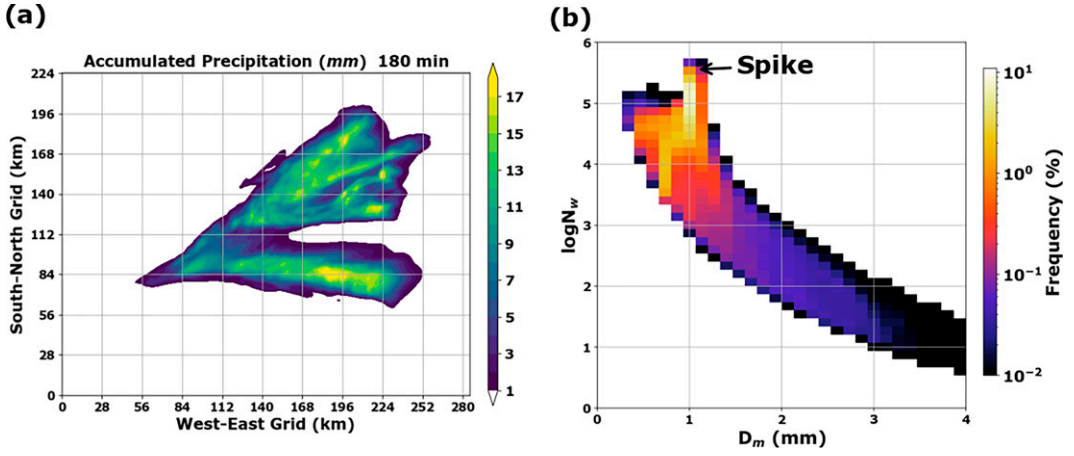

FIG. 2. From the RAMS supercell simulation: (a) accumulated precipitation and (b) raindrop D_m frequency distribution in logN_w–D_m phase space.

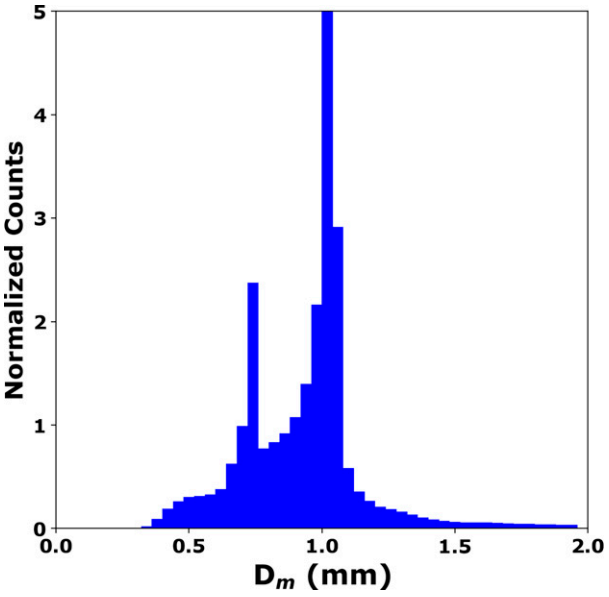

FIG. 3. Raindrop D_m frequency distribution (RDFD) represented as normalized bin counts of rain D_m across a range of size bins from the RAMS-2M supercell simulation. The counted data include grid cells in the lowest model layer to consider only raindrops impacting surface rainfall accumulation.

impact the raindrop DSD, the drop self-collisional breakup parameterization is the primary cause of the spike, as will be demonstrated below.

3. Raindrop breakup

a. *RAMS drop breakup parameterization*

The raindrop breakup parameterization in the RAMS microphysics scheme follows Verlinde et al. (1990) and VC93, and it is guided by disdrometer observations of ZA88. These observations were used to assist in the development of the VC93 raindrop self-collection efficiency equation. The ZA88 observations, from tropical Brazil, measured DSDs over varying rain rates from rainfall systems whose precipitation characteristics resemble that of deep convection. Their observations indicate that an equilibrium exists between collisional growth of drops and collisional drop breakup. Their equilibrium DSDs indicate an overall peak in distribution frequency for drops with diameter $D \sim 1.1$ mm, and secondary peaks at $D \sim 0.6$ and 2.0 mm. Seifert et al. (2005) cite the observational study of ZA88 (regarding equilibrium rain DSDs) as a good benchmark for assessing simulated collisional breakup parameterizations. More recently, D'Adderio et al. (2018) also noted that an equilibrium drop distribution is persistent for higher precipitation rates in deep convection, but that for nonconvective precipitation, processes other than breakup have a large influence and can prevent equilibrium. However, we should note that for the lighter rain scenarios included in the RAMS archived analysis, D_m rarely exceeded 1.0 mm, and thus breakup would be minimal via the VC93 formulation.

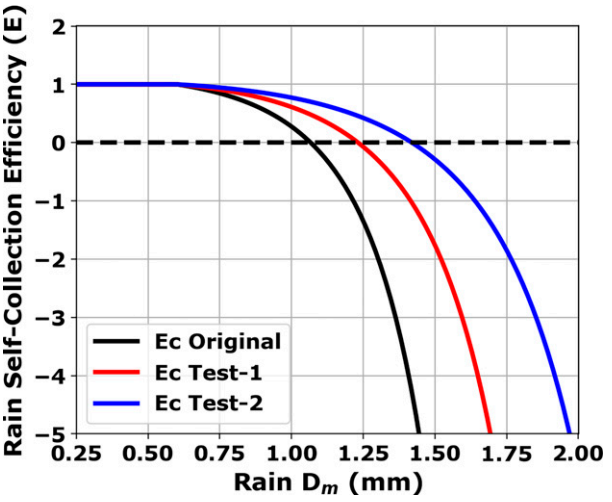

FIG. 4. Raindrop self-collection efficiency curves (E_c) relative to the raindrop distribution volume-number mean diameter (D_m). The black line depicts the default E_c in RAMS. The red and blue lines are experimental curves that delay drop breakup until drops grow to larger sizes. Drops begin to break up when the $E_c < 0$. The horizontal dashed line highlights the $E_c = 0$ point for each curve.

Drop breakup in RAMS is simulated through self-collection of raindrops via the collection efficiency (E_c) term. The current raindrop self-collection efficiency curve used is a minor modification of that presented in VC93. It is shown as the black curve in Fig. 4 and is given as

$$E_c = 1, \quad D_m < D_{\text{th}}, \tag{3}$$

$$E_c = 2 - \exp[A(D_m - D_{\text{th}})], \quad D_m \geq D_{\text{th}}, \tag{4}$$

where A (collection efficiency factor) = 1485 m^{-1}, D_m is the volume-number mean diameter of rain (as noted above), and D_{th} (0.6 mm) is the associated threshold mean diameter for breakup. It is evident from Fig. 4 that for D_m less than D_{th}, $E_c = 1$, thus leading to increased mean drop sizes and reduced drop numbers. For D_m between 0.6 and 1.07 mm, E_c is decreased exponentially to zero and hence the growth by self-collection is reduced. For D_m larger than 1.07 mm, E_c becomes negative and leads to drop breakup by adding number concentration to the raindrop hydrometeor category, thereby reducing D_m. A seemingly arbitrary minimum value of $E_c = -5$ is applied to limit excessive breakup; this minimum value of E_c will be addressed below with respect to possible modifications toward limiting breakup rates.

b. *Testing drop breakup in RAMS*

To assess the impact that the RAMS raindrop breakup parameterization may exert on the raindrop size and frequency distribution, we introduced modified raindrop self-collection efficiencies as shown by the red and blue curves in Fig. 4. These modified curves were chosen to expand the exponential curve so that it becomes negative at larger D_m. The baseline

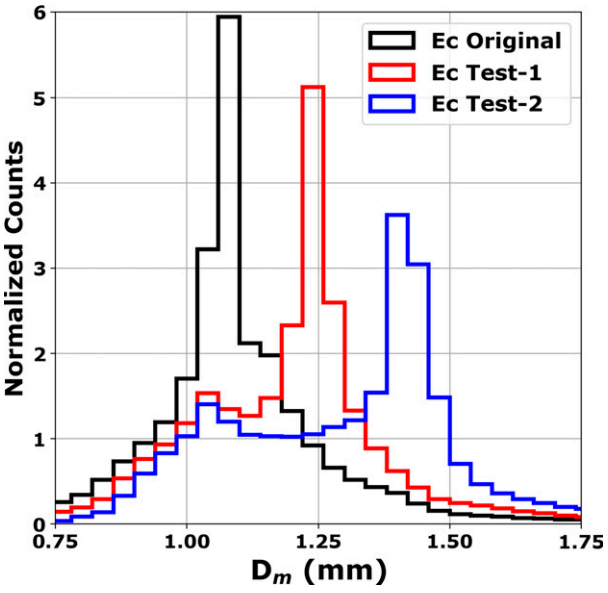

FIG. 5. Normalized counts of surface rain DSDs over a given range in D_m from RAMS supercell test simulations. The three distributions coincide with the raindrop self-collection equations for E_c in Fig. 4. Bin widths are 0.04 mm.

black curve (original, $A = 1485\ \mathrm{m}^{-1}$) crosses the $E_c = 0$ threshold at ~1.1 mm (slightly modified VC93) while the red (test 1, $A = 1097\ \mathrm{m}^{-1}$) and blue (test 2, $A = 845\ \mathrm{m}^{-1}$) curves cross $E_c = 0$ at ~ 1.24 and 1.40 mm, respectively. The resulting RDFDs from the RAMS supercell test simulations, associated with these varying representations of E_c, are shown in Fig. 5. In each simulation, there is a distinct peak in the RDFD that is associated with the diameter at which the curve of E_c becomes negative (indicating drop breakup). The peaks are also reduced in magnitude as their associated distributions broaden. As mentioned in VC93, the mean drop diameter, D_m, will tend to oscillate around the diameter at which $E_c = 0$, and settle at an equilibrium diameter that is near that size. Given the direct linkage between the diameter at which the spike is present in the $\log N_w$–D_m plots and the peak in the plots of RDFD in the control simulation, as well as the clear response in the peaks of the RDFD tests cases to varying E_c, it is highly likely that an overly efficient representation of raindrop breakup is the cause of the spikes in the previous figures of raindrop $\log N_w$–D_m. This is consistent with McTaggart-Cowan and List (1975), whereby they noted that coalescence and collisional breakup may be the two most dominant controls in the rain DSD.

4. Model intercomparisons of drop breakup

To determine if the distinct peak in the plots of RDFD are unique to the use of the RAMS bulk microphysics scheme, additional supercell simulations were performed using the Hebrew University Cloud Model with spectral bin microphysics (HUCM) (Khain et al. 2004) interfaced to RAMS (Igel and van den Heever 2017), as well as the Weather Research and Forecasting (WRF) Model version 3.9.1 (Skamarock 2006) using the Thompson (Thompson et al. 2004, 2008; Thompson and Eidhammer 2014), Morrison (Morrison et al. 2005, 2009, 2012), WRF double-moment 6-class (WDM6) (Lim and Hong 2010), and National Severe Storms Laboratory (NSSL) (Mansell et al. 2010) double-moment microphysics schemes. For the remainder of the discussion, these microphysics schemes, which are summarized in Table 3, will be identified by their namesakes or abbreviations without repetitive citation.

The additional supercell simulations using HUCM, Thompson, Morrison, WDM6, and NSSL microphysics schemes were run with the same grid configuration and initialization (see Table 2) as the RAMS simulations. (One difference from Table 1 for the WRF Model simulations is the use of a 1.5-order TKE turbulence parameterization.) While the RAMS and WRF parent models differ in numerous ways, the goal here is to assess if the various microphysics schemes generate a similar spike in raindrop $\log N_w$–D_m phase space and a peak in the RDFD, while also considering that general model variability can account for some of the differences. Default settings were used for each microphysics scheme tested herein. We recognize that various assumptions regarding single-moment versus double-moment approaches as well as the choice of raindrop size distribution type (e.g., inverse exponential versus gamma versus multimodal distributions) can influence the calculated diameters and the shape of the $\log N_w$–D_m frequency distribution and, thus, may impact the comparison to disdrometer observations.

TABLE 3. Summary of the microphysics schemes used in drop breakup intercomparison.

Parent model	Interfaced microphysics scheme	Drop breakup parameterization
RAMS	RAMS double-moment bulk (RAMS) (Verlinde et al. 1990; Walko et al. 1995; Meyers et al. 1997; Walko et al. 2000; Saleeby and Cotton 2004; Saleeby and van den Heever 2013)	Modified VC93
RAMS	Hebrew University Cloud Model–spectral bin microphysics (HUCM) (Khain et al. 2004; Seifert et al. 2005; Igel and van den Heever 2017)	Modified LL82
WRF	Morrison double-moment bulk (Morrison) (Morrison et al. 2005, 2009, 2012)	Modified VC93
WRF	Thompson double-moment bulk (Thompson) (Thompson et al. 2004, 2008; Thompson and Eidhammer 2014)	Modified VC93
WRF	WRF double-moment 6-class bulk (WDM6) (Lim and Hong 2010)	Modified VC93
WRF	National Severe Storms Laboratory double-moment bulk (NSSL) (Mansell et al. 2010; Ziegler 1985)	Modified BR74 + Modified LL82

Likewise, many of the physical parameterizations within each microphysics scheme may contribute to the convergence of raindrops at an equilibrium drop diameter, including autoconversion and accretion, melting of ice, raindrop breakup, and falling-hydrometeor size sorting. However, as demonstrated above for the example from the RAMS model, drop breakup parameterizations are applied indiscriminately to the resulting drop distributions and they act to limit excessive drop growth. While keeping in mind these model limitations as well as the variability in processes that impact the rain DSD, we seek to determine if other commonly used models and microphysics schemes generate similar frequency distributions of raindrop D_m and to highlight differences and similarities among the results from the various schemes. Given the strong linkage between simulated raindrop breakup and the peaks in RDFD, the drop breakup parameterizations, associated with each of the tested microphysics schemes, are briefly summarized below.

a. HUCM drop breakup

HUCM simulates droplet self-collection using stochastic collection (Bleck 1970) with the coalescence efficiencies of Beard and Ochs (1995). Within this method, self-collisional drop breakup is represented by the method of LL82. The details of this breakup parameterization are given in Seifert et al. (2005). The drop self-collection in HUCM uses a combination of several coalescence efficiencies (E_c) over various size ranges. For larger drops, they rely upon the laboratory data of LL82 that involved collisions between 10 drop pairs. E_c from LL82 is an empirical function of collision kinetic energy and surface energy of colliding drop pairs [Seifert et al. 2005, Eq. (5)]. A modification for collisions involving large drops ($D > 1.8$ mm) is applied from Brown (1997).

b. Thompson, Morrison, and WDM6 drop breakup

The Thompson, Morrison, and WDM6 microphysics schemes employ drop breakup parameterizations that rely upon the representation of E_c for raindrop collisional breakup that are similar to VC93 used in RAMS. In each scheme's drop breakup parameterization, the number concentration of raindrops is increased via the use of $E_c < 0$ to represent raindrop collisional breakup. The methods differ slightly in the details. The Thompson and Morrison schemes both use Eqs. (3) and (4) as they are presented here, but the Thompson scheme uses $D_{\text{th}} = 1.6$ mm (as the raindrop median volume diameter) and the Morrison scheme uses $D_{\text{th}} = 0.3$ mm (as the raindrop number-weighted mean diameter). Both schemes apply a weighting factor to the number of drops generated via self-collection collisional breakup. For raindrop exponential distributions in the default Thompson and Morrison schemes, their reported values of D_{th} are not dissimilar when expressed in the same rain mean/median diameter framework. WDM6 applies Eqs. (3) and (4) slightly differently than RAMS with respect to the representation of drop self-collection, but it uses the same basis of Eq. (4) for drop breakup such that the threshold diameter ($D_{\text{th}} = 0.6$ mm, volume-number mean diameter) is the same as that used in RAMS. However, WDM6 uses a collection efficiency factor $A = 2500\ \text{m}^{-1}$. This slightly modifies the representation of the self-collection efficiency curve compared to RAMS, but the essence and method of representing drop breakup is nearly the same. In summary, the RAMS, Thompson, Morrison, and WDM2 methods for representing drop self-collection and breakup use the same basic principles but include modifications to the collection efficiency curves.

c. NSSL drop breakup

The NSSL scheme parameterizes drop breakup following Mansell et al. (2010) and Ziegler (1985), which discuss drop breakup within the context of drop self-collection as represented by BR74. Within this self-collection method, drop breakup is represented in a similar manner to the previously mentioned parameterizations, such that the formulation of E_c considers the reduction in collisions of large drops as a means of preventing the formation of unrealistically large drops. Their specific formulation of E_c follows LL82 regarding the sizes of the most frequently colliding drop pairs and reduces E_c to 0 for a mean drop radius of 1 mm.

d. Simulation intercomparison of RDFD

Though not shown, all the supercell simulations, using RAMS, HUCM, Thompson, Morrison, WDM6, and NSSL microphysics schemes, generate splitting supercells with various amounts of accumulated surface precipitation. The RDFD for each supercell simulation using the various microphysics schemes is shown in Fig. 6. In this case, the RDFD is normalized such that the area under each curve equals one. Note first that the sharpest peaks with distinct cutoffs in RDFD occur in the simulations using the Thompson and WDM6 schemes. RAMS also has a sharp peak and does not generate many instances with $D_m > 1.25$ mm. The Morrison scheme also generates a sharp peak, but the curve is broader and permits more instances with larger D_m when compared with RAMS. These four schemes mentioned are those using the modifications of VC93 that permits $E_c < 0$ beyond a custom rain D_m threshold. The locations of the peaks are associated with the chosen thresholds and self-collection efficiency curves as discussed in VC93 and Planche et al. (2019). As mentioned earlier, these peaks are typically tuned to various cited observations as a means of choosing the most reliable value that works in conjunction with the other microphysical parameterizations in the respective schemes. The HUCM and NSSL schemes, both of which make use of the observations of colliding drop pairs in LL82, tend to have broader peaks in the RDFD. They also tend to favor a smaller peak frequency D_m, with a peak $D_m \sim 0.7$ mm for HUCM and $D_m \sim 0.4$ mm for NSSL. While individual rain DSDs shown in LL82 and Barros et al. (2008) are not directly comparable to the D_m frequency distributions shown here, we should note that the parameterizations associated with these studies of drop pair collisions, including more recently refined work (e.g., McFarquhar 2004; Schlottke et al. 2010; Straub et al. 2010; Prat et al. 2012), present a smaller modal diameter in the rain DSD compared to ZA88 (and thus the VC93 parameterization). This may account for the differences in the peak frequencies in D_m between

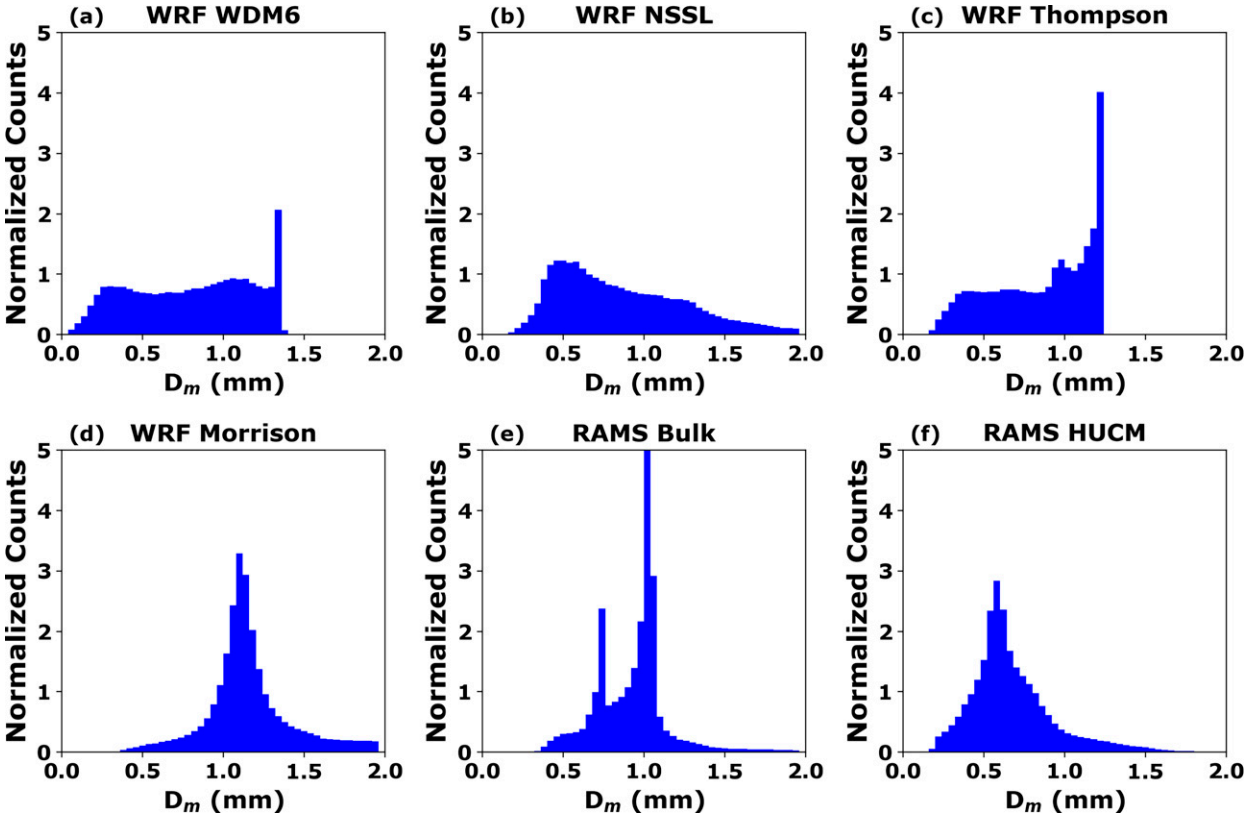

FIG. 6. Normalized raindrop D_m frequency distributions (RDFD) from supercell simulations using the various models and microphysics schemes shown in the legend. The counted data include grid cells in the lowest model layer to consider only rain impacting surface rainfall accumulation. Bin widths are 0.04 mm.

the models using these different base parameterizations of drop breakup.

The D_m frequency distribution is also shown in $\log N_w$–D_m phase space in Fig. 7 for the supercell simulations generated from the various microphysics schemes. There are several key features to note (that are not necessarily tied to drop breakup), some of which mimic the distributions seen in Fig. 6:

1) The Thompson and WDM6 schemes appear to have distinct rain D_m upper limits, near $D_m \sim 1.25$. DSDs with D_m beyond these cutoff sizes are not produced. Such general hydrometeor constraints are put in place by microphysics developers of two-moment schemes to help preserve a balance between hydrometeor mass and number. In spite of these upper bounds, these schemes capture the large majority of the $\log N_w$–D_m frequency distribution seen in the disdrometer observations from two convective cases (in Figs. 9e and 9f).
2) The RAMS and Morrison schemes permit the largest D_m (that approach 4 mm), although the frequency of occurrence of D_m larger than 3 mm is very low. Such large D_m drop distributions likely results from melted hail, but they are short-lived below the melting level as the drop breakup parameterizations force breakup into smaller drops. RAMS and Morrison also display the greatest frequency of occurrence near 1 mm diameter and a spike of larger $\log N_w$ at this size, though, the spike in the Morrison simulation is less pronounced than in RAMS. Experiments by Planche et al. (2019) suggest that the Morrison scheme provides better agreement to observations when using a smaller equilibrium threshold diameter.
3) The HUCM D_m frequency of occurrence is greatest near 0.6 mm diameter as also evident in Fig. 6. This most frequent D_m is substantially smaller than the frequently observed equilibrium drop size of 1 mm (ZA88; Dolan et al. 2018), which suggests that accretion and collisional growth are either too weak, or breakup is too strong in this scheme.
4) The WDM6, Thompson, and NSSL schemes all generate some grid cells with very high concentrations (high max $\log N_w$) of small D_m. In contrast, RAMS, HUCM and Morrison all have more limited small D_m number concentrations (lower max $\log N_w$) that fall more within the range of $\log N_w$ seen in the disdrometer observations associated with deep convection (Figs. 9e,f). As noted earlier, though, the disdrometer observations are limited in their detection of very small drops, and thus, may not be representing the smallest drop D_m produced in some of the simulations (e.g., Kathiravelu et al. 2016; Tokay et al. 2013). Furthermore, specific parameterizations and/or different delineations between cloud droplet and raindrop mean sizes in these schemes may permit formation of very small rain D_m.

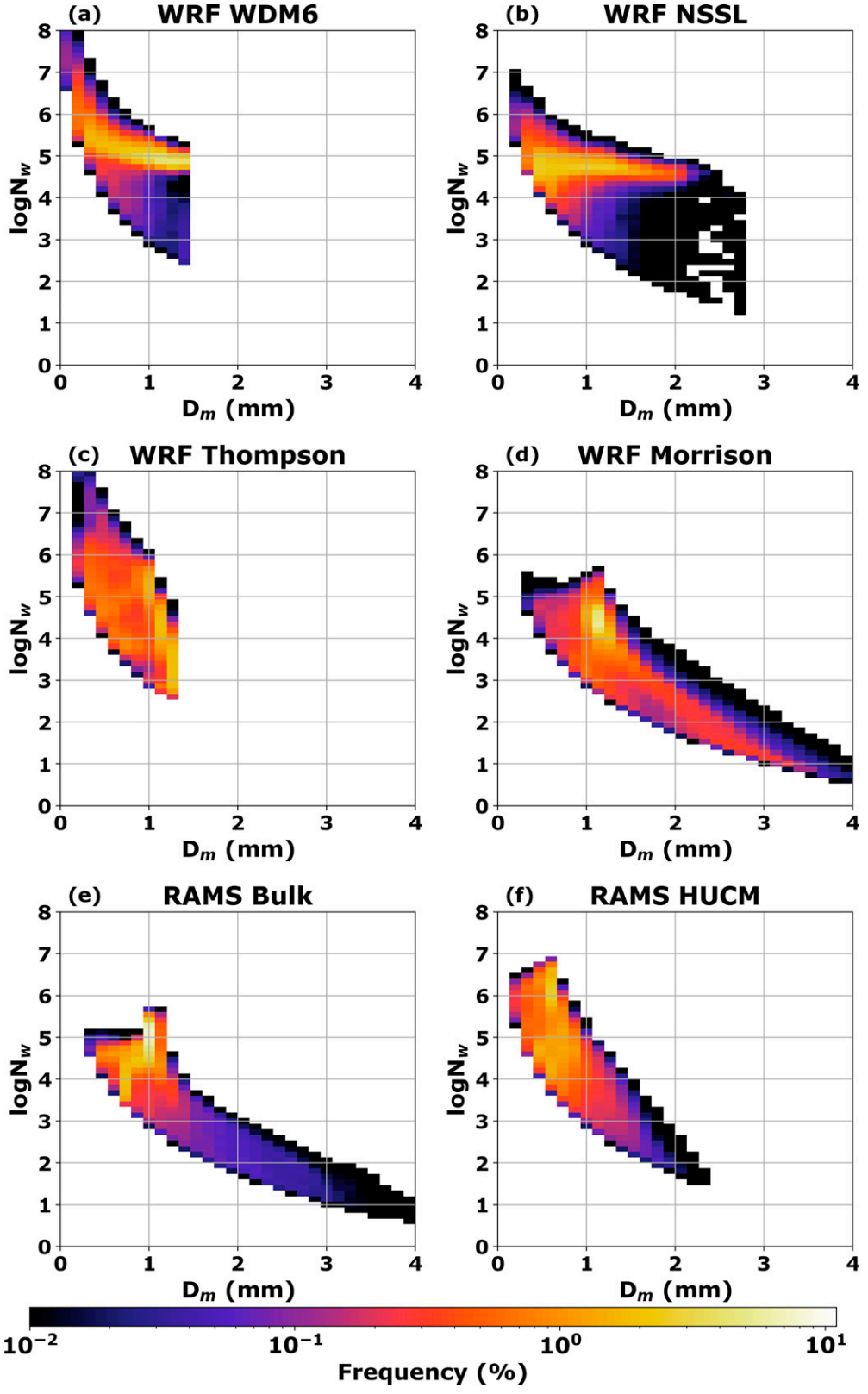

FIG. 7. Lowest-model-level raindrop logN_w–D_m frequency distribution from the high-resolution supercell simulation using the various model microphysics schemes tested in this study.

Each microphysics scheme generates a raindrop distribution, in $\log N_w$–D_m phase space, with its own unique set of constraints that shapes the range in the $\log N_w$ and D_m dimensions in this phase space (Fig. 7). In the disdrometer observations, the zone with peak frequency of occurrence tends to fall within a D_m range from ~0.50 to 1.25 mm and $\log N_w$ range from 3 to 5 ($\mathrm{mm}^{-1}\ \mathrm{m}^{-3}$). Most of the schemes tested in Fig. 7 have peak frequencies that largely fall in this range, suggesting that, in a broad sense, they are representing the rain DSD in a reasonable manner. However, there are various "spikes" or similar linear trends in the modeled $\log N_w$–D_m frequency distributions that are not seen in the equivalent disdrometer plots. It is important to note that numerous processes associated with each microphysics scheme contribute to the DSDs shown in Fig. 7. Differences in the assumed rain DSD shape parameters, drop size sorting, ice processes and subsequent melting to rain, as well as differences in warm-phase drop growth, all contribute to the final D_m frequency distributions. Each microphysics scheme has an array of parameterized processes that exert varying degrees of control over the final DSDs produced, as discussed for the Thompson and Morrison schemes in Planche et al. (2019). Our goal in this brief comparison among the schemes shown in Fig. 7 was to see if other microphysics schemes produce similar $\log N_w$–D_m raindrop frequency distributions to that seen from RAMS. While we were able to determine that the "spike" seen in RAMS $\log N_w$–D_m distribution is directly linked to the drop breakup parameterization, a more exhaustive investigation would be necessary to determine the dominant controls on the unique features of each microphysics scheme's $\log N_w$–D_m distribution.

A "spike" type feature is clearly present in the RAMS results and is marginally present in the Morrison results. As discussed early, experiments with the Morrison drop breakup parameterization have been performed via changes to the threshold breakup diameter (Planche et al. 2019). In the section that follows, we will explore a method of potentially reducing the "spike" seen in the RAMS results by reducing the strength of drop breakup without modifying the threshold diameter established in VC93.

5. Adjusting raindrop breakup parameterizations

Given the limited laboratory studies (e.g., LL82; Barros et al. 2008) on which to formulate physically based parameterizations of drop breakup, modelers sometimes need to fine-tune parameterizations of breakup to keep drop sizes within a reasonable range (VC93; Morrison et al. 2012; Planche et al. 2019). Of the WRF schemes that use the VC93 approach, the primary method of tuning has been related to the value of the raindrop self-collection threshold diameter; this diameter has been modified to obtain better agreement with observed number concentrations of raindrops (i.e., Morrison et al. 2012; Planche et al. 2019). Tuning can be dependent upon the microphysics scheme since various parameterized processes can impact raindrop number concentration and diameter, as highlighted in Planche et al. (2019). Thus, no single cited tuned value can necessarily be applied to other microphysics parameterizations.

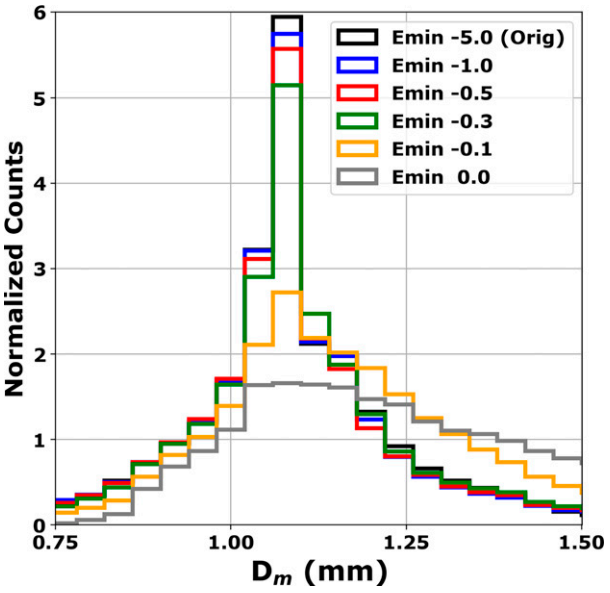

FIG. 8. Normalized counts of rain D_m from RAMS supercell test simulations. The counted data include grid cells in the lowest model layer to consider only raindrops impacting surface rainfall accumulation. The curves depict simulations with varying application of minimum collection efficiency (E_c). "$E_{\min}$ −5.0 (Orig)" required $E_c > -5$, while simulation "$E_{\min}$ −1.0" required $E_c > -1.0$, and so forth for the remaining experiments. Bin widths are 0.04 mm.

Another method of refining the VC93 parameterization of drop breakup involves applying limits to the maximum breakup rate, as determined by the minimum self-collection efficiency $E_{\min}$, while retaining the equilibrium drop diameter at which $E_c = 0$. This type of tuning should limit the strength of the drop breakup process while keeping the equilibrium size in close agreement to ZA88. Since the RAMS model exhibits the most prominent spike and highest frequency of occurrence at the equilibrium drop size (Fig. 7), it was used for testing modifications to the maximum breakup rate via changes to the $E_{\min}$ parameter. However, the results shown here could also be applied to other microphysics schemes using a similar drop breakup parameterization.

Drop breakup test simulations were performed with RAMS using various values of the minimum drop self-collection efficiency, $E_{\min}$, as applied from VC93. Recall that more negative values of $E_{\min}$ produce more efficient drop breakup. In these tests, $E_{\min}$ was varied incrementally from −5.0 (default in RAMS), toward the less negative values of −1.0, −0.5, −0.3, −0.1, and 0.0.

Figure 4 displays a minimum ordinate value of −5 corresponding with RAMS default $E_{\min} = -5.0$. In the test where $E_{\min} = -1.0$, for example, the collection efficiency curve is the same as the black line in Fig. 4, but with the ordinate minimum truncated at $E_c = -1.0$. Figure 8 displays plots of RDFD from these test simulations. It reveals a reduction in the height of the peak in RDFD as $E_{\min}$ becomes less and less

negative (moving from −5.0 to 0.0), with the most noticeable change occurring for a change in E_{min} from −0.3 to −0.1. It may be inferred from this figure that drop breakup is still quite active for relatively small negative values of E_{min}. For an $E_{min} = 0.0$, there is still a peak in RDFD near 1.0 mm, but the D_m frequency distribution is broader.

The use of $E_{min} = 0.0$ is akin to that described for the NSSL scheme that does not use negative values of E_c. The NSSL plot of RDFD is quite broad (Fig. 6) as is the RDFD plot for the RAMS test simulation with $E_{min} = 0.0$. The main difference between these two scenarios is the location of the D_m peak. NSSL generates a propensity toward $D_m \sim 0.4$ mm (Fig. 6) while RAMS with $E_{min} = 0.0$ produces the greatest occurrence of drops at $D_m \sim 1$ mm (Fig. 8). Again, the greatest occurrence of D_m is controlled by the threshold diameters in the formulations of E_c as well as the diameter where $E_c = 0$, and these are generally tuned with respect to the parent microphysics scheme.

Plots of $\log N_w$–D_m for these supercell tests with varying E_{min} are shown in Figs. 9a–d. For comparison to observations, Figs. 9e and 9f display the results of disdrometer data from the iFloodS and MC3E field campaigns, both of which included deep isolated and organized convection. While we should not necessarily expect the supercell test results to exactly match those from these specific field campaign data, we can make some broad comparisons with regards to the range of expected drop sizes found in deep convection and the size drops with the greatest frequency of occurrence. Figure 9 demonstrates that a reduction in the drop breakup strength, controlled by changing E_{min} from −5.0 to 0.0, leads to 1) a reduction in the spike near 1 mm D_m, 2) greater frequency of occurrence of larger D_m, and 3) a broader peak in the higher frequency D_m denoted as a larger area of orange shaded pixels. The test with $E_{min} = 0.0$ offers, perhaps, too great of a reduction in drop breakup. Figure 9d depicts a distribution that still has its peak near 1 mm, but the diagonal shape of the distribution is somewhat lost in comparison to the disdrometer distributions and the other tests of E_{min}. While additional testing is necessary to determine an optimal and less ad hoc value of the E_{min} parameter in this drop self-collection parameterization, it appears that a reduction in the maximum allowed strength in the raindrop breakup parameterization does help reduce the persistence of the artificial spike of high frequency of occurrence of large $\log N_w$ at $D_m \sim 1$ mm. Perhaps a combination of modified E_{min} and a reduction in the breakup threshold diameter [similar to that tested in Planche et al. (2019) for the Thompson and Morrison schemes] would provide additional improvements.

6. Summary and conclusions

In this study we have compared the raindrop size distributions, in $\log N_w$–D_m phase space, from a global disdrometer database to an extensive database of RAMS model simulations composed of tropical, maritime, shallow, and deep precipitating cloud systems. Here D_m is the volume-number mean diameter of the raindrop gamma DSD and N_w is the intercept parameter. It was noted that the simulations tended to produce 1) a narrower range of D_m than in the observations, 2) a lower frequency of D_m from 1.0 to 1.5 mm than observed, and 3) a "spike" of high $\log N_w$ of rain DSD with $D_m \sim 1$ mm diameter that is not evident in the observations. It was found that this spike was most prevalent in simulations of deep convection, where, in reality, drops can grow to appreciable size through vigorous collision–coalescence processes and melting of large ice particles.

Model experimentation revealed that the parameterization of raindrop self-collisional breakup was the cause of the persistent occurrence of rain with $D_m \sim 1$ mm at high $\log N_w$. While other microphysical processes certainly contribute to the prediction of drop size, it was shown that the VC93 parameterization of drop breakup exerts a strong control on the mean drop size via the assignment of the threshold drop diameter and the assigned maximum strength of drop breakup via negative collection efficiencies.

Given that many microphysics schemes in numerical models use similar approaches to parameterize raindrop collisional breakup, a set of comparative numerical simulations of deep convection (idealized supercell) were run using different models and microphysics schemes as summarized in Table 3. These include the double-moment bulk microphysics schemes from RAMS, WRF-Thompson, WRF-Morrison, WRF-WDM6, and WRF-NSSL, as well as the HUCM-Bin scheme interfaced to the RAMS dynamic model. Analysis of the raindrop size distributions in $\log N_w$–D_m phase space from these simulations (Fig. 7) reveals that nearly all the model results display a degree of numerical constraint while broadly agreeing with the zone of peak frequencies in the $\log N_w$–D_m disdrometer observations (Figs. 1a, 9e,f). The apparent constraints vary, however, by microphysics scheme and may not always be clearly linked to the parameterization of drop breakup. For example, the rain D_m distribution from the WRF-Thompson and WRF-WDM6 simulations (Figs. 6, 7) display hard upper bounds and do not permit D_m beyond ~1.3 mm in diameter. Meanwhile, the remainder of the microphysics schemes permit some D_m beyond this threshold. However, the disdrometer frequency distributions do not reveal many occurrences of $D_m > 1.5$ mm, though this could be due to the upper size limits of drop detection and subsequent fitting to gamma distributions.

Each of the microphysics schemes using a derivative of the VC93 approach to drop breakup (RAMS, WRF-Thompson, WRF-Morrison, WRF-WDM6) all exhibit sharp peaks in the rain D_m frequency distribution (Fig. 6) with the most frequently occurring D_m near 1 mm, as is formulated in the VC93 parameterization. The most prolific rain D_m from the WRF-NSSL and HUCM-Bin schemes occurs near 0.5–0.6 mm (Fig. 6). Both WRF-NSSL and HUCM use the LL82 drop breakup approach based on observed colliding drop pairs, though WRF-NSSL applies a breakup limitation such that the drop self-collection efficiency, E_c does not drop below zero. VC93 permits $E_c < 0$, with breakup becoming more efficient for increasingly negative values. This suggests that limiting the settings of E_c to values closer to zero, rather than more negative minimum values, may allow a VC93 type of breakup parameterization to reduce the forcing of large drops to $D_m \sim 1$ mm.

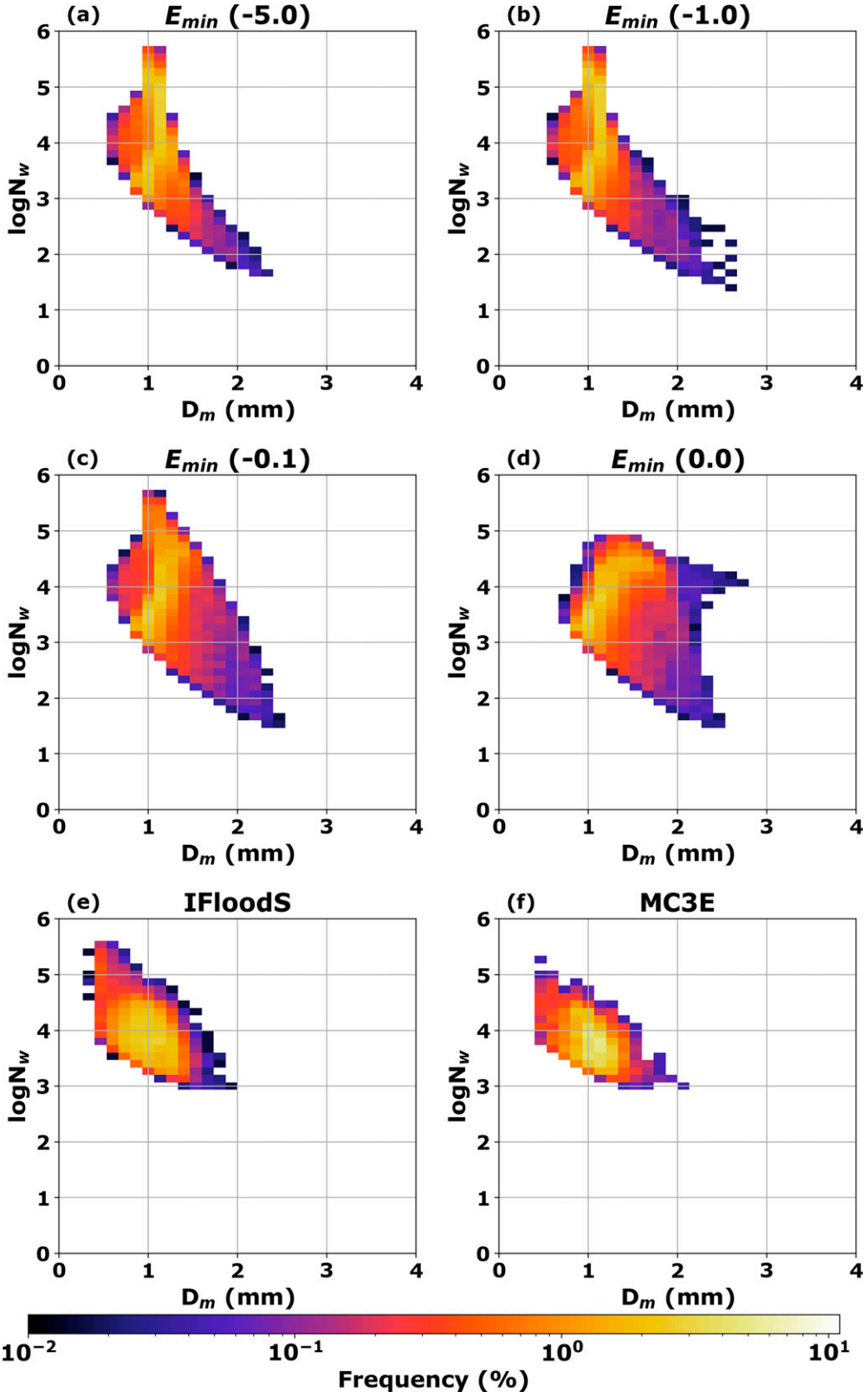

FIG. 9. (a)–(d) Lowest-model-level raindrop logN_w–D_m frequency distribution from the RAMS supercell test simulations with varying raindrop minimum negative self-collection efficiency $E_{\min}$. (e),(f) As in (a)–(d), but from disdrometer observations from the IFloodS and MC3E fields projects, respectively.

To investigate this possibility, supercell test simulations were run with the RAMS microphysics with perturbations to the minimum value to E_c ($E_{\min}$). These tests used the same simulation setup as those that were run to isolate the microphysical process(es) responsible for the "spike" in high $\log N_w$ for $D_m \sim 1$ mm. In the VC93 drop breakup application in RAMS, an arbitrary value of $E_{\min} = -5$ is set. Recall that WRF-NSSL uses $E_{\min} = 0.0$ (in combination with the LL82 approach). In this set of test simulations, $E_{\min}$ was varied from 0 to −5. Figures 8 and 9 indicate that as $E_{\min}$ is modified from −5 to 0 (becoming less negative), the "spike" becomes less prominent. While these figures cannot definitively determine the optimal value of $E_{\min}$ to use in the VC93 parameterization in the RAMS microphysics, values of $E_{\min}$ closer toward $E_{\min} = 0.0$ (though, perhaps, not $E_{\min} = 0.0$ itself) do provide a drop size trend that is more comparable to the general disdrometer observations. In the future, direct case study comparisons between disdrometer observations and model simulations could provide a more quantitative determination of the optimal upper limit to apply to drop breakup in microphysics schemes that parameterize breakup as VC93.

Acknowledgments. This work was supported by the Department of Energy under Grant DE-SC0017977.

Data availability statement. The datasets from the suite of numerical simulations and global disdrometers on which this paper is based is too large to be retained or publicly archived with available resources. Model and instrument output as well as documentation and methods used to support this study are available from the manuscript authors at Colorado State University Department of Atmospheric Science. The archive of the available files and tools related to the analyses herein is available at https://doi.org/10.25675/10217/235397.

REFERENCES

Barros, A. P., O. P. Prat, P. Shrestha, F. Y. Testik, and L. F. Bliven, 2008: Revisiting Low and List (1982): Evaluation of raindrop collision parameterizations using laboratory observations and modeling. *J. Atmos. Sci.*, **65**, 2983–2993, https://doi.org/10.1175/2008JAS2630.1.

Beard, K. V., and H. T. Ochs, 1995: Collisions between small precipitation drops. Part II: Formulas for coalescence, temporary coalescence, and satellites. *J. Atmos. Sci.*, **52**, 3977–3996, https://doi.org/10.1175/1520-0469(1995)052<3977:CBSPDP>2.0.CO;2.

Berry, E. X., and R. L. Reinhardt, 1974: An analysis of cloud drop growth by collection: Part I. Double distributions. *J. Atmos. Sci.*, **31**, 1814–1824, https://doi.org/10.1175/1520-0469(1974)031<1814:AAOCDG>2.0.CO;2.

Bleck, R., 1970: A fast, approximative method for integrating the stochastic coalescence equation. *J. Geophys. Res.*, **75**, 5165–5171, https://doi.org/10.1029/JC075i027p05165.

Brown, B. R., M. M. Bell, and G. Thompson, 2017: Improvements to the snow melting process in a partially double moment microphysics parameterization. *J. Adv. Model. Earth Syst.*, **9**, 1150–1166, https://doi.org/10.1002/2016MS000892.

Brown, P. S., 1997: Mass conservation considerations in analytic representation of raindrop fragment distributions. *J. Atmos. Sci.*, **54**, 1675–1687, https://doi.org/10.1175/1520-0469(1997)054<1675:MCCIAR>2.0.CO;2.

Cotton, W. R., and Coauthors, 2003: RAMS 2001: Current status and future directions. *Meteor. Atmos. Phys.*, **82**, 5–29, https://doi.org/10.1007/s00703-001-0584-9.

D'Adderio, L. P., F. Porcù, and A. Tokay, 2018: Evolution of drop size distribution in natural rain. *Atmos. Res.*, **200**, 70–76, https://doi.org/10.1016/j.atmosres.2017.10.003.

Dolan, B., B. Fuchs, S. A. Rutledge, E. A. Barnes, and E. J. Thompson, 2018: Primary modes of global drop-size distributions. *J. Atmos. Sci.*, **75**, 1453–1476, https://doi.org/10.1175/JAS-D-17-0242.1.

Gatlin, P. N., M. Thurai, V. N. Bringi, W. Petersen, D. Wolff, A. Tokay, L. Carey, and M. Wingo, 2015: Searching for large raindrops: A global summary of two-dimensional video disdrometer observations. *J. Appl. Meteor. Climatol.*, **54**, 1069–1089, https://doi.org/10.1175/JAMC-D-14-0089.1.

Grant, L. D., and S. C. van den Heever, 2014a: Microphysical and dynamical characteristics of low-precipitation and classic supercells. *J. Atmos. Sci.*, **71**, 2604–2624, https://doi.org/10.1175/JAS-D-13-0261.1.

——, and ——, 2014b: Aerosol-cloud-land surface interactions within tropical sea breeze convection. *J. Geophys. Res. Atmos.*, **119**, 8340–8361, https://doi.org/10.1002/2014JD021912.

——, T. P. Lane, and S. C. van den Heever, 2018: The role of cold pools in tropical oceanic convective systems. *J. Atmos. Sci.*, **75**, 2615–2634, https://doi.org/10.1175/JAS-D-17-0352.1.

Igel, A. L., and S. C. van den Heever, 2017: The importance of the shape of cloud droplet size distributions in shallow cumulus clouds. Part I: Bin microphysics simulations. *J. Atmos. Sci.*, **74**, 249–258, https://doi.org/10.1175/JAS-D-15-0382.1.

Kathiravelu, G., T. Lucke, and P. Nichols, 2016: Rain drop measurement techniques: A review. *Water*, **8**, 29, https://doi.org/10.3390/w8010029.

Khain, A., A. Pokrovsky, M. Pinsky, A. Seifert, and V. Phillips, 2004: Simulation of effects of atmospheric aerosols on deep turbulent convective clouds using a spectral microphysics mixed-phase cumulus cloud model. Part I: Model description and possible applications. *J. Atmos. Sci.*, **61**, 2963–2982, https://doi.org/10.1175/JAS-3350.1.

Lim, K.-S. S., and S.-Y. Hong, 2010: Development of an effective double-moment cloud microphysics scheme with prognostic cloud condensation nuclei (CCN) for weather and climate models. *Mon. Wea. Rev.*, **138**, 1587–1612, https://doi.org/10.1175/2009MWR2968.1.

Low, T. B., and R. List, 1982: Collision, coalescence and breakup of raindrops. Part II: Parameterization of fragment size distributions. *J. Atmos. Sci.*, **39**, 1607–1619, https://doi.org/10.1175/1520-0469(1982)039<1607:CCABOR>2.0.CO;2.

Mansell, E. R., C. L. Ziegler, and E. C. Bruning, 2010: Simulated electrification of a small thunderstorm with two-moment bulk microphysics. *J. Atmos. Sci.*, **67**, 171–194, https://doi.org/10.1175/2009JAS2965.1.

Marinescu, P. J., S. C. van den Heever, S. M. Saleeby, and S. M. Kreidenweis, 2016: The microphysical contributions to and evolution of latent heating profiles in two MC3E MCSs. *J. Geophys. Res. Atmos.*, **121**, 7913–7935, https://doi.org/10.1002/2016JD024762.

McFarquhar, G. M., 2004: A new representation of collision-induced breakup of raindrops and its implications for the shapes of raindrop size distributions. *J. Atmos. Sci.*, **61**, 777–794,

https://doi.org/10.1175/1520-0469(2004)061<0777:ANROCB>2.0.CO;2.

McTaggart-Cowan, J. D., and R. List, 1975: Collision and breakup of water drops at terminal velocity. *J. Atmos. Sci.*, **32**, 1401–1411, https://doi.org/10.1175/1520-0469(1975)032<1401:CABOWD>2.0.CO;2.

Meyers, M. P., R. L. Walko, J. Y. Harrington, and W. R. Cotton, 1997: New RAMS cloud microphysics parameterization. Part II: The two-moment scheme. *Atmos. Res.*, **45**, 3–39, https://doi.org/10.1016/S0169-8095(97)00018-5.

Morrison, H., J. A. Curry, and V. I. Khvorostyanov, 2005: A new double-moment microphysics parameterization for application in cloud and climate models. Part I: Description. *J. Atmos. Sci.*, **62**, 1665–1677, https://doi.org/10.1175/JAS3446.1.

——, G. Thompson, and V. Tatarskii, 2009: Impact of cloud microphysics on the development of trailing stratiform precipitation in a simulated squall line: Comparison of one- and two-moment schemes. *Mon. Wea. Rev.*, **137**, 991–1007, https://doi.org/10.1175/2008MWR2556.1.

——, S. A. Tessendorf, K. Ikeda, and G. Thompson, 2012: Sensitivity of a simulated midlatitude squall line to parameterization of raindrop breakup. *Mon. Wea. Rev.*, **140**, 2437–2460, https://doi.org/10.1175/MWR-D-11-00283.1.

Planche, C., F. Tridon, S. Banson, G. Thompson, M. Monier, A. Battaglia, and W. Wobrock, 2019: On the realism of the rain microphysics representation of a squall line in the WRF Model. Part II: Sensitivity studies on the rain drop size distributions. *Mon. Wea. Rev.*, **147**, 2811–2825, https://doi.org/10.1175/MWR-D-18-0019.1.

Prat, O. P., A. P. Barros, and F. Y. Testik, 2012: On the influence of raindrop collision outcomes on equilibrium drop size distributions. *J. Atmos. Sci.*, **69**, 1534–1546, https://doi.org/10.1175/JAS-D-11-0192.1.

Pruppacher, H. R., and J. D. Klett, 1997: *Microphysics of Clouds and Precipitation*. 2nd ed. Kluwer Academic, 954 pp.

Saleeby, S. M., and W. R. Cotton, 2004: A large-droplet mode and prognostic number concentration of cloud droplets in the Colorado State University Regional Atmospheric Modeling System (RAMS). Part I: Module descriptions and supercell test simulations. *J. Appl. Meteor.*, **43**, 182–195, https://doi.org/10.1175/1520-0450(2004)043<0182:ALMAPN>2.0.CO;2.

——, and S. C. van den Heever, 2013: Developments in the CSU-RAMS aerosol model: Emissions, nucleation, regeneration, deposition, and radiation. *J. Appl. Meteor. Climatol.*, **52**, 2601–2622, https://doi.org/10.1175/JAMC-D-12-0312.1.

——, C. H. Twohy, S. C. van den Heever, and P. J. DeMott, 2011: Impacts of Saharan dust on the microphysical processes in tropical convection. *2011 Fall Meeting*, San Francisco, CA, Amer. Geophys. Union, A11C-0107, https://abstractsearch.agu.org/meetings/2011/FM/A11C-0107.html.

——, S. R. Herbener, S. C. van den Heever, and T. L'Ecuyer, 2015: Impacts of cloud droplet–nucleating aerosols on shallow tropical convection. *J. Atmos. Sci.*, **72**, 1369–1385, https://doi.org/10.1175/JAS-D-14-0153.1.

Schlottke, J., W. Straub, K. D. Beheng, H. Gomaa, and B. Weigand, 2010: Numerical investigation of collision-induced breakup of raindrops. Part I: Methodology and dependencies on collision energy and eccentricity. *J. Atmos. Sci.*, **67**, 557–575, https://doi.org/10.1175/2009JAS3174.1.

Seifert, A., A. Khain, U. Blahak, and K. D. Beheng, 2005: Possible effects of collisional breakup on mixed-phase deep convection simulated by a spectral (bin) cloud model. *J. Atmos. Sci.*, **62**, 1917–1931, https://doi.org/10.1175/JAS3432.1.

Skamarock, W. C., 2006: Positive-definite and monotonic limiters for unrestricted-time-step transport schemes. *Mon. Wea. Rev.*, **134**, 2241–2250, https://doi.org/10.1175/MWR3170.1.

Smagorinsky, J., 1963: General circulation experiments with the primitive equations. *Mon. Wea. Rev.*, **91**, 99–164, https://doi.org/10.1175/1520-0493(1963)091<0099:GCEWTP>2.3.CO;2.

Smith, P. L., Z. Liu, and J. Joss, 1993: A study of sampling-variability effects in raindrop size observations. *J. Appl. Meteor.*, **32**, 1259–1269, https://doi.org/10.1175/1520-0450(1993)032<1259:ASOSVE>2.0.CO;2.

Straub, W., K. D. Beheng, A. Seifert, J. Schlottke, and B. Weigand, 2010: Numerical investigation of collision-induced breakup of raindrops. Part II: Parameterizations of coalescence efficiencies and fragment size distributions. *J. Atmos. Sci.*, **67**, 576–588, https://doi.org/10.1175/2009JAS3175.1.

Thompson, E. J., S. A. Rutledge, B. Dolan, and M. Thurai, 2015: Drop size distributions and radar observations of convective and stratiform rain over the equatorial Indian and west Pacific Oceans. *J. Atmos. Sci.*, **72**, 4091–4125, https://doi.org/10.1175/JAS-D-14-0206.1.

Thompson, G., and T. Eidhammer, 2014: A study of aerosol impacts on clouds and precipitation development in a large winter cyclone. *J. Atmos. Sci.*, **71**, 3636–3658, https://doi.org/10.1175/JAS-D-13-0305.1.

——, R. M. Rasmussen, and K. Manning, 2004: Explicit forecasts of winter precipitation using an improved bulk microphysics scheme. Part I: Description and sensitivity analysis. *Mon. Wea. Rev.*, **132**, 519–542, https://doi.org/10.1175/1520-0493(2004)132<0519:EFOWPU>2.0.CO;2.

——, P. R. Field, R. M. Rasmussen, and W. D. Hall, 2008: Explicit forecasts of winter precipitation using an improved bulk microphysics scheme. Part II: Implementation of a new snow parameterization. *Mon. Wea. Rev.*, **136**, 5095–5115, https://doi.org/10.1175/2008MWR2387.1.

Tokay, A., A. Kruger, and W. F. Krajewski, 2001: Comparison of drop size distribution measurements by impact and optical disdrometers. *J. Appl. Meteor.*, **40**, 2083–2097, https://doi.org/10.1175/1520-0450(2001)040<2083:CODSDM>2.0.CO;2.

——, W. A. Petersen, P. Gatlin, and M. Wingo, 2013: Comparison of raindrop size distribution measurements by collocated disdrometers. *J. Atmos. Oceanic Technol.*, **30**, 1672–1690, https://doi.org/10.1175/JTECH-D-12-00163.1.

Toms, B. A., S. C. van den Heever, E. M. Riley Dellaripa, S. M. Saleeby, and E. D. Maloney, 2020: The boreal summer Madden–Julian oscillation and moist convective morphology over the Maritime Continent. *J. Atmos. Sci.*, **77**, 647–667, https://doi.org/10.1175/JAS-D-19-0029.1.

Tzivion, S., G. Feingold, and Z. Levin, 1987: An efficient numerical solution to the stochastic collection equation. *J. Atmos. Sci.*, **44**, 3139–3149, https://doi.org/10.1175/1520-0469(1987)044<3139:AENSTT>2.0.CO;2.

Verlinde, J., and W. R. Cotton, 1993: Fitting microphysical observations of nonsteady convective clouds to a numerical model: An application of the adjoint technique of data assimilation to a kinematic model. *Mon. Wea. Rev.*, **121**, 2776–2793, https://doi.org/10.1175/1520-0493(1993)121<2776:FMOONC>2.0.CO;2.

——, P. J. Flatau, and W. R. Cotton, 1990: Analytical solutions to the collection growth equation: Comparison with approximate methods and application to cloud microphysics parameterization schemes. *J. Atmos. Sci.*, **47**, 2871–2880, https://doi.org/10.1175/1520-0469(1990)047<2871:ASTTCG>2.0.CO;2.

Walko, R. L., W. R. Cotton, M. P. Meyers, and J. Y. Harrington, 1995: New RAMS cloud microphysics parameterization part I: The single-moment scheme. *Atmos. Res.*, **38**, 29–62, https://doi.org/10.1016/0169-8095(94)00087-T.

——, ——, G. Feingold, and B. Stevens, 2000: Efficient computation of vapor and heat diffusion between hydrometeors in a numerical model. *Atmos. Res.*, **53**, 171–183, https://doi.org/10.1016/S0169-8095(99)00044-7.

Williams, C. R., and Coauthors, 2014: Describing the shape of raindrop size distributions using uncorrelated raindrop mass spectrum parameters. *J. Appl. Meteor. Climatol.*, **53**, 1282–1296, https://doi.org/10.1175/JAMC-D-13-076.1.

Zawadzki, I., and M. De Agostinho Antonio, 1988: Equilibrium raindrop size distributions in tropical rain. *J. Atmos. Sci.*, **45**, 3452–3459, https://doi.org/10.1175/1520-0469(1988)045<3452:ERSDIT>2.0.CO;2.

Ziegler, C. L., 1985: Retrieval of thermal and microphysical variables in observed convective storms. Part 1: Model development and preliminary testing. *J. Atmos. Sci.*, **42**, 1487–1509, https://doi.org/10.1175/1520-0469(1985)042<1487:ROTAMV>2.0.CO;2.